Steel and Composite Structures, *Vol. 56, No. 5 (2025) 393-404*
https://doi.org/10.12989/scs.2025.56.5.393

Nonlinear finite element modeling of timber scarf joints with and without steel pins

Hafshah Salamah[1], Goangseup Zi[2], Jong-Sub Lee[2] and Thomas H.-K. Kang[*3]

[1]*Department of Architecture, Institute of Technology Bandung, Ganeca 10 Bandung, Indonesia*
[2]*Department of Civil, Environmental and Architectural Engineering, Korea University, 145 Anam-ro, Seongbuk-gu, Seoul 02841, Korea*
[3]*Department of Architecture and Architectural Engineering, Seoul National University, 1 Gwanak-ro, Gwanak-gu, Seoul 08826, Korea*

(Received January 28, 2025, Revised March 23, 2025, Accepted March 26, 2025)

Abstract. This study numerically evaluates the behavior of timber scarf joints with and without steel pins using finite element models across various parameters. Three-dimensional (3D) nonlinear finite element models were developed based on a micro-modeling approach to examine their response to static loads. Experimental results were used to calibrate and validate the numerical models. Experimental results were used to calibrate and validate the numerical models. Sensitivity analysis revealed that the material properties of the scarf members were the most critical factor in achieving strong connections, surpassing the influence of key or dowel members. Simulation accuracy improved with smaller mesh sizes, increased load increments, and more iterations, though at the expense of higher complexity and longer computation times. Parametric analysis provided deeper insights into scarf joint behavior under tension and compression loads parallel to the grain. Analysis on the geometric parameter revealed that the basic size proportions recommended in the literature provide the best combination, offering greater strength compared to other size combinations. Additionally, timber scarf joints were analyzed with varying numbers of steel or wooden dowels, focusing on identifying the impact of the dowel to scarf joints. This study highlights the potential of using numerical modeling to evaluate scarf joints, while acknowledging the limitations of the tools.

Keywords: finite element model; parametric analysis; scarf joint; steel pin; traditional timber connection

1. Introduction

A scarf joint is a type of carpentry joint used to join two elements lengthwise. Due to its shape and ability to resist tension loads parallel to wood grain, it is classified as a tension joint. This joint is also known as *bitgeoli-ieum* in Korean traditional timber joint types (National Research Institute of Cultural Heritage in Korea 2014) and as *sambungan bibir miring* in Indonesian traditional joinery. It is commonly used for beam-to-beam connections, such as rafters in floor structures (Fig. 1) or roof structures.

The form of scarf joint exhibit distinct characteristics, featuring diagonal contact surfaces and typically being constructed from harder wood to ensure a tight fit and ease of application. There are several variations of scarf joints, but the most common ones in traditional buildings are (a) the stop-splayed scarf joint and (b) the stop-splayed and tabled scarf joint with a key (Karolak *et al*. 2020) (Fig. 2).

As one of the most common traditional timber joints, understanding the behavior of scarf joints in traditional buildings is important. Structural evaluation is essential for preserving these joints and preventing failure, as well as for gaining knowledge about their performance. Based on Branco and Descamps (2015), the assessment of joint behavior depends on several key factors: (1) the mechanical properties of the wood, (2) determining stiffness and load-bearing capacity, (3) evaluating compression stresses in contact zones, and (4) analyzing the distribution of shear stresses in the joints. In this study, these aspects will be evaluated in scarf joints using three-dimensional finite element model analysis. Several types of scarf joints will be examined to verify the interaction between key parameters and characteristics within the model settings.

Fig. 1 Scarf joint in floor structure on Nuwo Sesat, traditional building in Indonesia

A comprehensive study on timber scarf joints was conducted by Ceraldi *et al*. (2021), providing an insightful analysis comparing basic scarf joints, scarf joints with wooden dowels, and scarf joints with metal dowels to basic metal dowel connections. Research on scarf joints remains

*Corresponding author, Professor
E-mail: tkang@snu.ac.kr

ISSN: 1229-9367 (Print), 1598-6233 (Online)

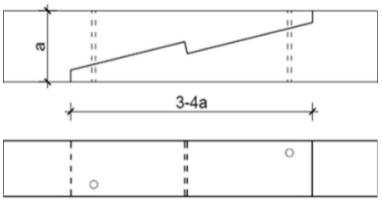

(a) Stop-splayed scarf joint

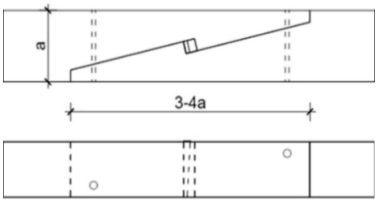

(b) Stop-splayed and tabled scarf joint with key

Fig. 2 Variants of timber scarf joint (adapted from Karolak *et al*. 2020)

limited, particularly regarding their capacity in wooden structures. Most studies on traditional timber joints have focused on mortise-tenon and dovetail joints, especially their lateral or seismic performance (Li *et al*. 2020, Yang *et al*. 2020, Xue *et al*. 2021, Feio *et al*. 2014, Emile *et al*. 2018).

Other joint types primarily explore the flexural or rotational behavior of the connections. Wu *et al*. (2022) performed compression force tests to analyze bracket joints through numerical and analytical methods. Ren *et al*. (2021) examined the rotational performance of cross-shaped mortise-tenon joints, both with and without dowels, through experimental and theoretical analyses. Their findings showed that mortise-tenon joints with dowels exhibited higher ductility compared to those without. Schmidt and Daniels (1999) studied mortise-tenon connections and developed strength equations based on various failure modes. Although these studies provide valuable data on mortise-tenon joints, they mostly remain at the experimental phase and have not been widely replicated or implemented.

Among studies on traditional timber joints, some have used finite element analysis (FEA) to compare numerical and experimental results. Xue *et al*. (2020) performed precise FEA of full-scale straight-tenon joints, and Li *et al*. (2020) studied Chinese mortise and tenon joints. Li *et al*. (2015) conducted seismic performance tests on a double-span traditional timber frame, validating their findings with a two-dimensional finite element model (FEM). Sha *et al*. (2019) also performed FEA on a traditional Chinese timber frame under cyclic loads, comparing the results with experimental data. Li *et al*. (2015) demonstrated a significant convergence between FEA and experimental results, indicating that both two-dimensional and three-dimensional FEA can provide valuable insights for structural analysis.

This study consists of two main stages of analysis: (1) validation and sensitivity analysis of numerical modeling, and (2) parametric studies of scarf joints. Stage one involves validating the numerical model for scarf joints to determine the feasibility of structural analysis using

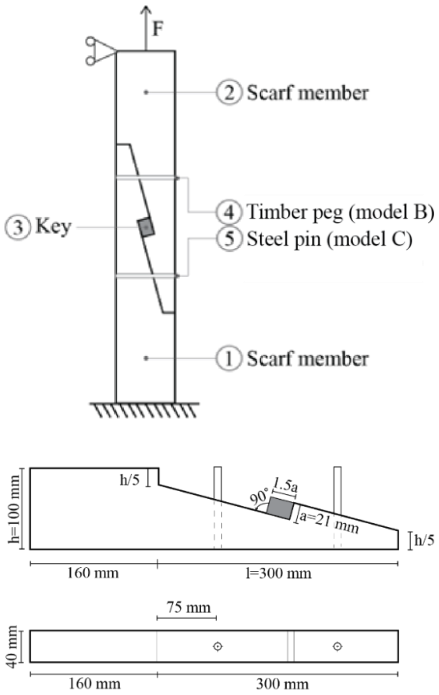

Fig. 3 Design set-up

numerical methods and to assess how closely the results align with experimental data. Sensitivity analysis was also conducted to identify the optimal model configuration, enhancing the accuracy of the simulation. In stage two, the basic scarf joint is evaluated under different parameters to identify the most influential factors affecting the connection. As the parametric study focuses on the effects of parameter changes, the accuracy of the results is less critical and primarily serves as a reference for improving scarf joint performance in building structures. Due to study limitations, material properties from wood testing were not used; instead, assumptions from the literature were adopted to achieve more precise simulation results aligned with experimental findings.

2. Validation of numerical modeling

2.1 Material and models

There are three models of scarf joint for the validation stage: Model A represents a basic scarf joint, Model B includes scarf joints with two wooden pegs, and Model C with two steel pins (Fig. 3). Both the wooden pegs and steel pins used had a diameter of 8 millimeters each. These models were adapted from the specimens used in the experimental work conducted by Ceraldi *et al*. (2021). Finite element analysis (FEA) was employed for the numerical modeling of scarf joints using RFEM software by Dlubal, in accordance with the Eurocode 5 standard.

The material axis orientation was adjusted according to the orthotropic properties of wood. In RFEM, the longitudinal direction aligns with the x-axis, the radial direction with the y-axis, and the tangential direction with the z-axis. The wood material properties for the FEA were

Table 1 Mechanical properties for numerical model

Material	Strength properties (MPa)						Poisson's ratio				Mean density (ρ) (kg/m^3)
	Bending ($f_{m,k}$)	Tensile		Compression		Shear	μ_{LR},	μ_{LT}	μ_{RT}	μ_{TR}	μ_{RL}, μ_{TL}	
		($f_{t,0,k}$)	($f_{t,90,k}$)	($f_{c,0,k}$)	($f_{c,90,k}$)	($f_{v,k}$)						
Ash (D40)	40	24	0.6	27	5.5	4.2	0.4	0.6	0.6	0.03	350
Fir (C30)	30	19	0.4	24	2.7	4	0.3	0.4	0.4	0.01	460

Note: '$f_{t,0,k}$', '$f_{t,90,k}$', '$f_{c,0,k}$', and '$f_{c,0,k}$' denote the tensile strength parallel to grain, tensile strength perpendicular to grain, compression strength parallel to grain, and compression strength perpendicular to grain, respectively. 'μ' denotes Poisson's ratio, while the subscripts of 'L', 'R', and 'T' denote longitudinal, radial, and tangential wood axis, respectively.

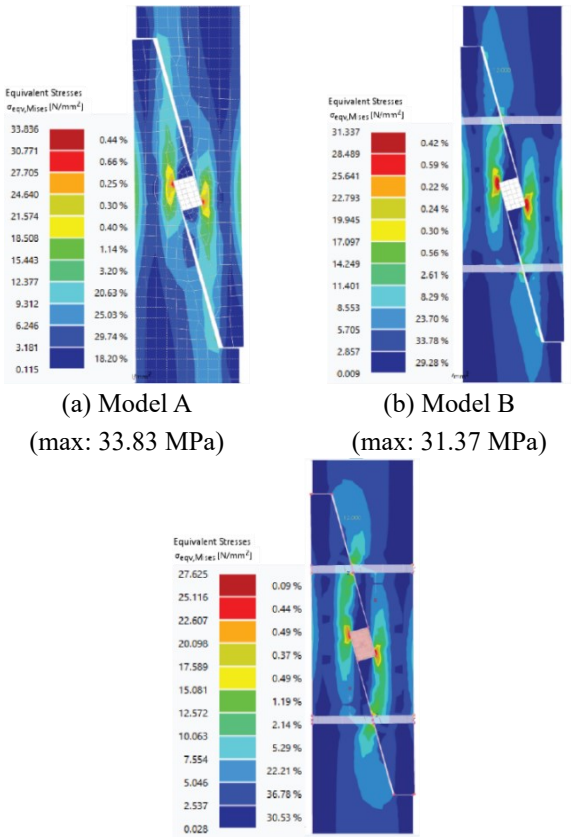

(a) Model A (max: 33.83 MPa) (b) Model B (max: 31.37 MPa)

(c) Model C (max: 27.62 MPa)

Fig. 4 Stress distribution of scarf joint members

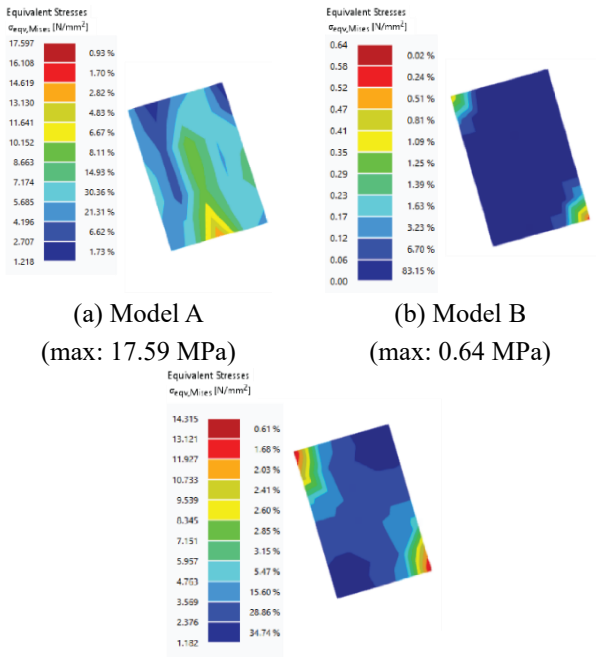

(a) Model A (max: 17.59 MPa) (b) Model B (max: 0.64 MPa)

(c) Model C (max: 14.31 MPa)

Fig. 5 Stress distribution on key components

selected according to the Eurocode 5 standard, aiming to match the material used in the experimental work by Ceraldi *et al*. (2021). Since only the material density was specified in their experiments, various assumptions regarding strength and stiffness properties had to be made to meet the requirements for numerical modeling. For the steel pins, AISI 316 steel with a yield strength of 200 MPa was used. D40 wood grade was chosen for the key elements, while C30 grade was used for the scarf members. Since Poisson's ratio for orthotropic materials is not automatically generated in RFEM, values were sourced from Mechanical Properties of Wood by the U.S. Department of Agriculture's Forest Service (Green *et al*. 1999) (Table 1).

The type of analysis selected for this model is 'Orthotropic Plastic' to capture nonlinear deformation in the simulation. The orthotropic plastic model in RFEM employs the Tsai-Wu failure criterion. Boundary conditions include a fixed surface at the base of the model and a roller support at the top of the joint to simulate the experimental clamp setup. A tensile force of 12 kN is applied to the middle of the top surface, in line with the experimental setup.

The control settings for the analysis are configured to 'Second Order (P-Δ) Picard,' with 100 iterations and a load increment of 200. The mesh size is set to 10 mm, utilizing a combination of triangular and quadrilateral elements.

2.2 FEA results and discussion

2.2.1 Stress distribution

All stress and strain distributions are determined using equivalent values derived from von Mises principles that closely approximate the Tsai-Wu failure criterion for timber materials. For the scarf members, due to their lower material strength compared to key or dowel members, they are more susceptible to failure than key or dowel members.

In Fig. 4, between Models A, B, and C, the area of

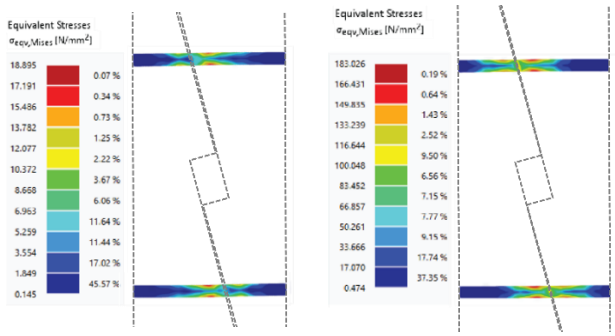

(a) Timber dowels in Model B (max: 18.89 MPa)

(b) Steel pins in Model C (max: 183.03 MPa)

Fig. 6 Stress distribution on dowel members

Table 2 Comparison between experimental and numerical yield load results

No	Type of model	Exp. result (kN)	Mean exp. result (kN)	Num. result (kN)	Error (%)
1	Model A	4.600 6.400	5.500	7.080	29%
2	Model B	6.400 8.500 7.800	7.560	9.240	22%
3	Model C	4.600 7.800 9.500	7.300	10.440	43%

Note: Experimental yield load results are taken from Ceraldi *et al*. (2021)

maximum stress in Model B is larger than in Models A and C. Given that the maximum compression strength of fir (C30) is 24 MPa, stress exceeding 24 MPa can be considered indicative of a failure state in the connection. The maximum values from three models indicate that in the simulation, Model B is more likely to fail in the scarf members than other members. Meanwhile, for the key members, the equivalent stress for Model A is seen spreading along the key members, while for Models B and C, stress concentrates at the edge of the key members within the scarf members. This suggests that dowels play a crucial role in preventing failures near the key member. The compression strength of 27 MPa for key members exceeds the maximum stress experienced by all key members in Models A, B, and C, indicating there are no failures on the key members (Fig. 5).

Only Models B and C incorporate dowel members in their setup. Due to differences in material, the behavior of the dowels varies when resisting tension loads. Both dowels experience primary stress at the contact points between the scarf members. In their stress distributions, each dowel exhibits significantly different maximum stress values: Model B at 18.895 MPa and Model C at 183.026 MPa (Fig. 6). Both values remain below the compression parallel to grain of D40 ash and the yield strength of S200, which are 27 MPa and 200 MPa, respectively.

The stress distributions indicate that the scarf members experience failures while the key and dowels remain within their maximum strength limits. This finding aligns with the failure modes recorded by Ceraldi *et al*. (2021), which suggests that all configurations of the scarf connection may primarily exhibit shear failures in the scarf members rather than in the key or dowel members. Other potential failure modes include crushing of the key in Models A and B, splitting across the grain of the key in Model B, and embedment failure in the key and dowels in Model C. However, these variations in failure modes can only be observed through experimental methods, which require multiple specimens and are limited in numerical simulations.

2.2.2 Load-displacement curve

From the numerical simulations, the load-displacement curve was obtained based on the load increments and maximum deformation values. The load increment was adjusted from the initial range of 0 to 200 to a range of 0 to 12 kN. To determine the yield load, the method outlined by Ceraldi *et al*. (2021) was followed. A straight line parallel to the linear phase of the diagram was plotted, maintaining the same difference between each increment value, and 5% of the 8 mm fastener diameter (0.4 mm) was added. This process continued until the intersection with the load-displacement curve was found, which was recorded as the yield point. The load-displacement diagram is shown in Fig. 7, with detailed values presented in Table 2.

It was observed that the yield point of Model A was lower than those of Models B and C. This indicates that the addition of dowels significantly enhances connection strength compared to basic scarf joints (Model A), with an increase of at least 31% for double wooden pegs and 47% for double steel pins. This indicates that relying solely on the key member is not sufficient to achieve a strong wood connection. Although the load-displacement diagram from the numerical analysis may not fully match the experimental results, the yield point obtained from the numerical simulation shows a 69% accuracy compared to the mean value from the experimental results.

It is important to note that the average yield load in the experimental results was derived from a broad range between the highest and lowest yielding samples, which may be influenced by unknown factors. The variability in experimental results was not explicitly explained by Ceraldi *et al*. (2021), suggesting two possible causes: human error and the inherent variability in timber material properties. Despite these differences, the numerical simulation provides valuable insights into the mechanical behavior of the connection, though it may not be as reliable as experimental data and requires further calibration.

2.2.3 Stiffness degradation curve

As the connections are subjected to increasing loads, they gradually undergo deformation, indicating a reduction in stiffness as the load increases. This stiffness degradation is crucial for understanding the behavior of the connection under load. From the load-deformation curve in the previous section, a stiffness degradation curve can be derived using Eq. (1) (Li *et al*. 2020, Emile *et al*. 2018).

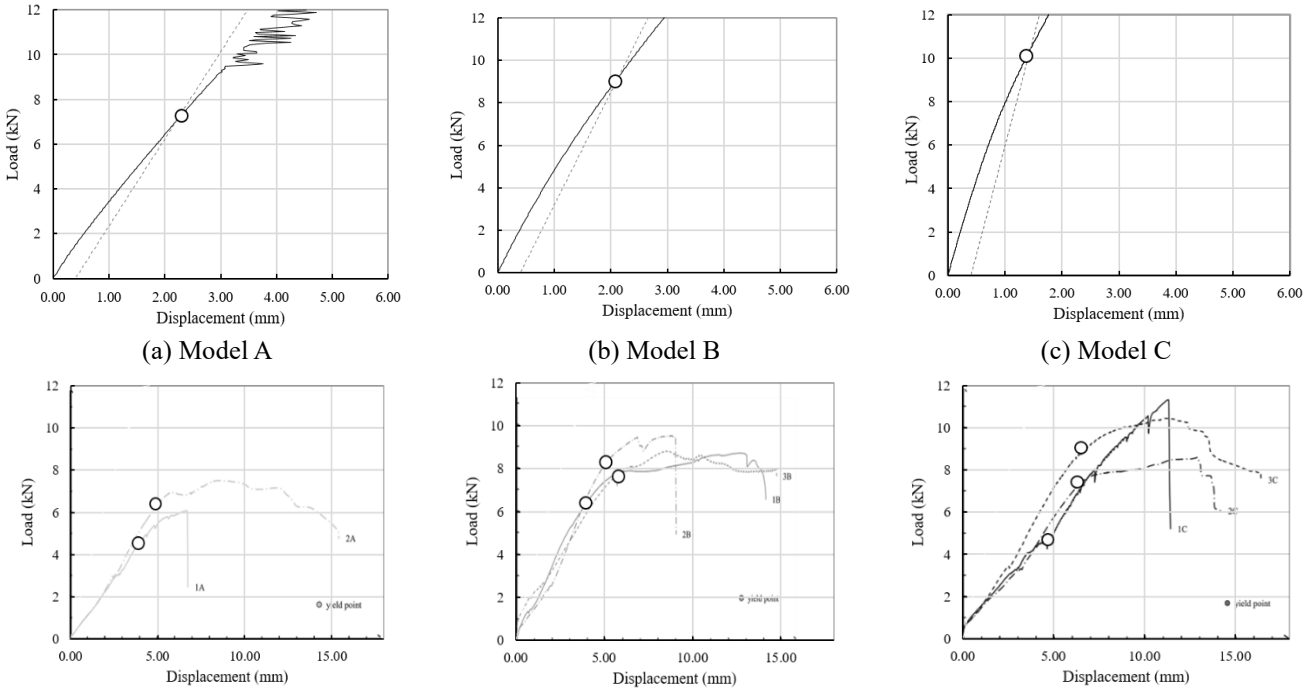

(a) Model A (b) Model B (c) Model C

(d) Sample A (e) Sample B (f) Sample C

Fig. 7 Load-displacement curves based on numerical and experimental results (diagrams of Samples A, B, and C are adapted from Ceraldi *et al*. (2021))

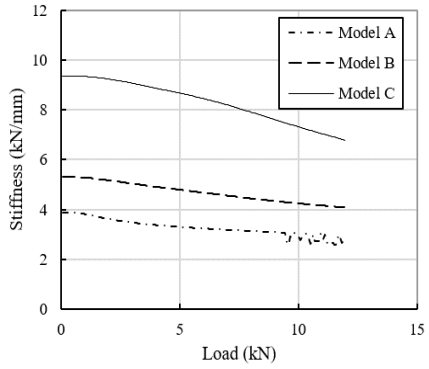

Fig. 8 Stiffness degradation curve of numerical model

$$K_i = \frac{|+F_i| + |-F_i|}{|+\Delta_i| + |-\Delta_i|} \quad (1)$$

where Δ_i, K_i, and F_i denote the control displacement, the lateral stiffness, and lateral force of the specimens under the grade i, respectively.

The stiffness degradation curve shown in Fig. 8 illustrates that each model maintains its stiffness at the onset of loading. However, after reaching 1 kN, the stiffness begins to steadily decrease as displacement increases, indicating the onset of degradation. Model C exhibits the highest initial stiffness among the models, while Model A shows lower stiffness than Model B values initially. Specifically, at the beginning of loading, Model A, Model B, and Model C exhibit stiffness values of 3.89 kN/mm, 5.30 kN/mm, and 9.36 kN/mm, respectively. Upon reaching a tension load of 12 kN, the stiffness decreases to 2.80 kN/mm for Model A, 4.08 kN/mm for Model B, and 6.79 kN/mm for Model C, representing reductions of 28%, 23%, and 27% from their initial stiffness values, respectively. Unexpectedly, despite Model C initially demonstrating superior stiffness, Model B exhibits higher stiffness retention over the course of loading compared to Models A and C. This finding offers valuable insights into the behavior of the connection under tension loads, highlighting the importance of further comparisons between experimental and numerical results.

3. Sensitivity analysis

Due to the numerous assumptions required for numerical modeling of timber scarf joints, a sensitivity analysis was conducted to identify the configuration that best aligns the numerical results with experimental data. Thus, Model B, scarf joint with wooden dowels, was chosen as the object of sensitivity analysis. The sensitivity analysis focused on variations in material strength categories and general settings within RFEM.

3.1 Material properties

The analysis was divided into two groups: (1) variations in the material grade of the scarf members, and (2) variations in the material grade of the key and dowel members. The parameter control for the models were C30 softwood for the scarf members and D40 for the key and dowel members, consistent with the numerical modeling outlined in the previous section. For the sensitivity analysis, nine additional material grades from the softwood category

Table 3 Strength properties for sensitivity analysis

Material	Strength properties (MPa)						Mean density (ρ) (kg/m^3)
	Bending ($f_{m,k}$)	Tensile		Compression		Shear	
		($f_{t,0,k}$)	($f_{t,90,k}$)	($f_{c,0,k}$)	($f_{c,90,k}$)	($f_{v,k}$)	
Hardwood – for dowel and key members							
D27	27	16	0.6	22	5.1	3.8	610
D35	35	21	0.6	25	5.4	4.1	650
D40 (control)	40	24	0.6	27	5.5	4.2	350
D45	45	27	0.6	29	5.8	4.4	700
D50	50	30	0.6	30	6.2	4.5	740
Softwood – for scarf members							
C22	22	13	0.4	20	2.4	3.8	410
C24	24	14.5	0.4	21	2.5	4	420
C30 (control)	30	19	0.4	24	2.7	4	460
C35	35	22.5	0.4	25	2.7	4	470
C40	40	26	0.4	27	2.8	4	480
C45	45	30	0.4	29	2.9	4	490

Note: '$f_{t,0,k}$', '$f_{t,90,k}$', '$f_{c,0,k}$', and '$f_{c,0,k}$' denote the tensile strength parallel to grain, tensile strength perpendicular to grain, compression strength parallel to grain, and compression strength perpendicular to grain, respectively.

Table 4 Strength properties for sensitivity analysis

Material grade	Displacement (mm)	Initial stiffness (kN/mm)	Stiffness at 12 kN (kN/mm)	Degradation	Yield load (kN)
C22	3.78	4.61	3.17	31%	7.200
C24	3.37	4.96	3.56	28%	7.920
C30 (control)	2.94	5.30	4.08	23%	9.240
C35	2.76	5.55	4.35	22%	9.840
C40	2.5	5.98	4.81	20%	10.920
C45	2.322	6.31	5.17	18%	11.400

were considered: C22, C24, C35, C40, and C45 for the scarf members; and D27, D35, D45, and D50 for the key and dowel members. All analyses were conducted under identical conditions, with 100 iterations and 100 load increments. The strength properties for each group are detailed in Table 3.

3.1.1 Various material grades for scarf members

For the sensitivity analysis for the scarf members, load-displacement and stiffness diagram are obtained and calculated from numerical modeling results. From the load-displacement diagram presented in Fig. 9, the displacement of the connection decreases significantly as the material grade increases (Table 4).

This phenomenon also affects the stiffness of the joints. The initial stiffness values for material grades increase as the material grade increases. Subsequently, the stiffness decreases as the applied load increases. The highest stiffness reduction is observed for scarf members with material grade C22, with a 31% reduction, while the lowest stiffness reduction is observed for scarf members with material grade C45, with an 18% reduction. This demonstrates that the higher material grades result in higher stiffness and greater resistance to loads compared to the lower grades. The yield load of the joints is also impacted by the material grade of the scarf member, with an increase observed as the material grade increases.

3.1.2 Various material grades for key and dowel members

There are not many differences observed in the displacement and stiffness when the material grade of the key and dowel members is changed. The yield load of the joints also remained the same at 9240 N. The displacement for the key and dowel members for D27 and D35 is the same at 2.9 mm, while for D40, D45, and D50 it is 3.0 mm (Fig. 10). Although there are slight differences in the initial and decreased stiffness for each material grade, the variations consistently hover around 29-30% (Table 5). This is likely due to the same failure mode primarily occurring in the scarf members rather than the key or dowel members. This phenomenon suggests that changes in the dowel material, if the scarf members remain within the same timber properties, will not have a significant impact on the stiffness and strength of the joint.

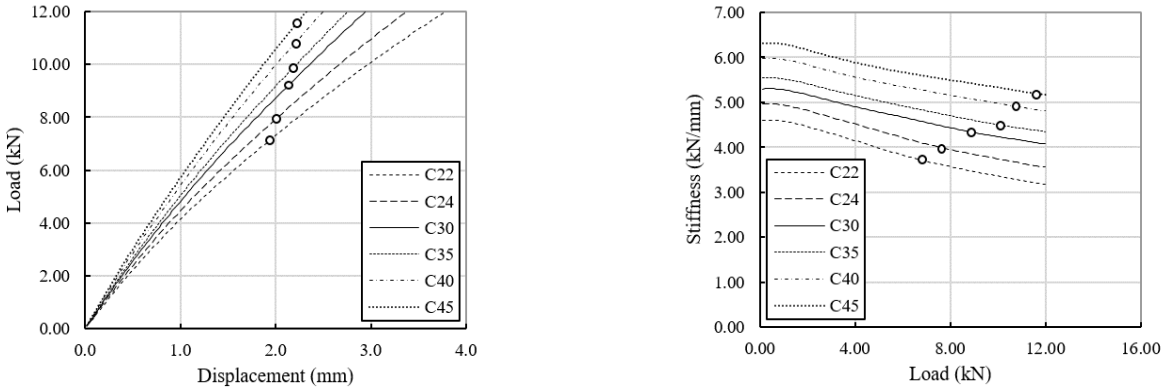

(a) (b)

Fig. 9 (a) Load-displacement curves and (b) stiffness degradation curves for various material grades of timber scarf members

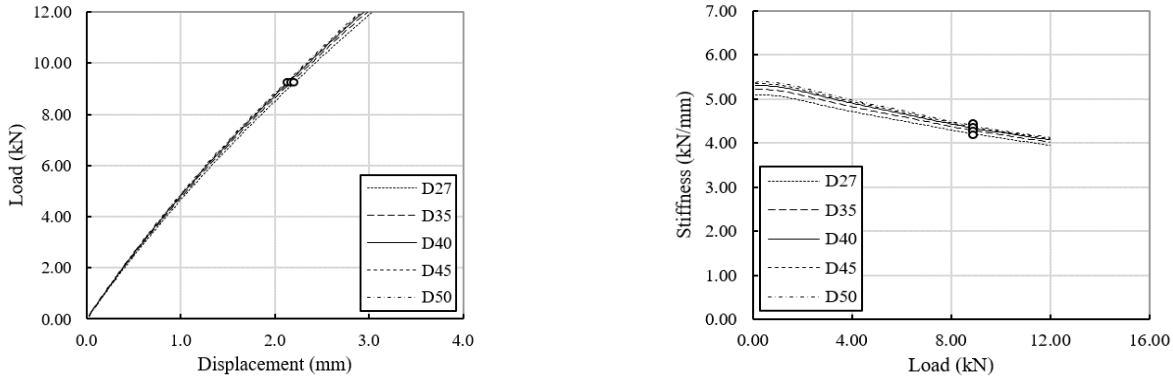

(a) (b)

Fig. 10 (a) Load-displacement curves and (b) stiffness degradation curves for various material grades of key and dowel members

3.2 Model analysis setting

The sensitivity analysis on the model settings was conducted by varying the mesh size, iteration count, and load increments. The scarf members were assigned the control material of C30, while the key and dowel members of D40 material grade.

3.2.1 Mesh size

The analysis of Model B with varying mesh sizes (5 mm, 10 mm, 15 mm, and 20 mm) reveals the substantial effect of mesh size on the accuracy of the connection (Fig. 11). While the key member retained a constant 4 mm mesh refinement, the rest of the model used larger mesh sizes. For mesh sizes of 15 mm and 20 mm, the yield load could not be determined due to the absence of an intersection between the 5% dowel diameter offset linear line and the displacement curve. Additionally, the stiffness observed with 15 mm and 20 mm mesh sizes was unrealistically high, exceeding the highest material strength of C45 from the earlier analysis.

Among the different mesh sizes, the 5 mm mesh provided a more accurate result, showing only a 14% error compared to the experimental results, whereas the 10 mm mesh exhibited a 22% error. The finer mesh sizes also impacted on the stiffness of the model, with stiffness decreasing as the mesh size became finer. This analysis highlights the importance of mesh size selection in finite element modeling, especially in ensuring accuracy in load-displacement behavior and stiffness measurements.

3.2.2 Load increment and iteration

The model utilizes a control parameter of mesh size in 10 mm, load increment of 200 and iteration of 100. For the load increment and iteration analysis, values of 100, 200, 300, and 400 were compared. From the load-displacement and stiffness degradation diagram, load increment slightly affects the results at values of 300 and 400. Load increments of 100 and 200 exhibit similar yield loads 9.240 kN and stiffness values of 4.08 kN/mm, while 300 and 400 show lower values closer to the experimental results. A load increment of 300 has yield load of 9.120 kN, while 400-load increment has 8.880 kN. Since the control load increment is 200, only from 300 load increments onwards increase the accuracy of the simulation in the yield load parameter. The differences between the load increments enhance the accuracy of the joints but require much more time to complete, which needs to be carefully considered.

In terms of iteration, increasing the iteration value does not significantly improve the accuracy of the result. The control parameter of iterations was 100 and the result has 22% error from the experimental result. When the iteration

Table 5 Mechanical behavior of scarf joints in various timber grades (key and dowel members)

Material grade	Displacement (mm)	Initial stiffness (kN/mm)	Stiffness at 12 kN (kN/mm)	Degradation	Yield load (kN)
D27	3.04	5.09	3.95	22%	9.240
D35	2.98	5.21	4.03	23%	9.240
D40 (control)	2.94	5.30	4.08	23%	9.240
D45	2.92	5.34	4.10	23%	9.240
D50	2.9	5.38	4.13	23%	9.240

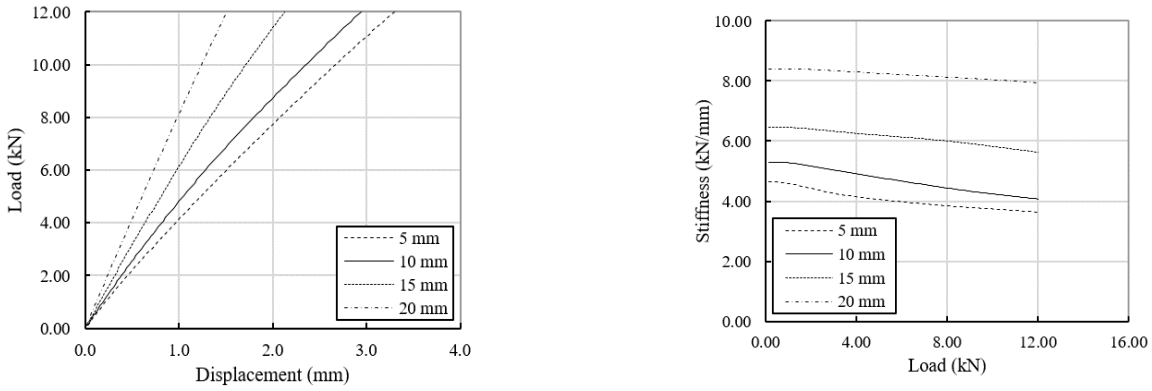

(a) (b)

Fig. 11 (a) Load-displacement curves and (b) stiffness degradation curves for various mesh sizes

is increased to 200, 300 and 400, the results are similar. The displacement increases to 3.0 mm, while the stiffness decreases from 5.22 kN/mm to 3.99 kN/mm, which is a 24% reduction from the original state. Additionally, the yield load decreases to 9000 N, which is a 19% deviation from the experimental result. Compared to the control model, this result presents more accuracy but requires more time to solve. However, since the results were similar for 200, 300, and 400 iterations, it can be concluded that 200 iterations are sufficient to obtain relatively accurate results.

From sensitivity analyses, material properties significantly impact connection strength, particularly in timber scarf members. For model analysis settings, a 5 mm mesh size, 400 load increment, and 200 iterations yield higher accuracy compared to experimental results. However, these settings are effective only for this specific model size and case. For further analysis, adjusting the model setting to the model size is essential to ensure accurate results.

4. Parametric analysis on scarf joints

In traditional timber joints, such as those used in Korean architecture, guidelines for the proportion and dimensions of joints are often recommended by institutions like the National Research Institute of Cultural Heritage. To further understand the behavior and performance of timber scarf joints, parametric analysis was conducted, focusing on geometry and dowel modifications. This parametric analysis provides valuable insights into the optimal configurations of scarf joints, helping to balance the historical preservation of traditional techniques with modern structural requirements. These findings can guide future timber construction projects, ensuring that scarf joints maintain both their aesthetic and structural integrity while meeting contemporary standards.

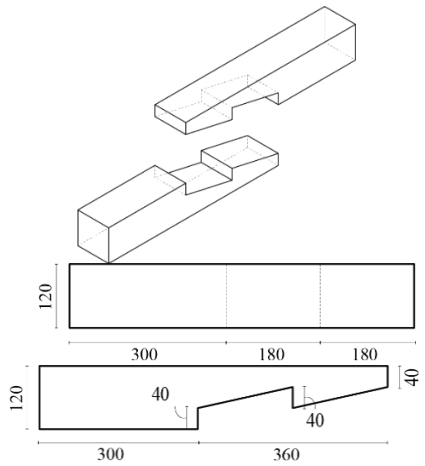

Fig. 12 Design setup for geometry modification analysis (unit: mm)

4.1 Geometry modifications

To better understand the factors influencing the performance of timber scarf joints, the basic configuration of a scarf joint without the inclusion of keys or dowels was selected for analysis (Fig. 12). This baseline model focuses on assessing the core joint itself, isolating the behavior of the joint geometry under load without additional

Table 6 Mechanical behavior of timber scarf joint under various joint lengths

Length (mm)	Displacement (mm)	Initial stiffness (kN/mm)	Stiffness degradation
Tension			
180	9.56	11.52	73%
240	7.43	13.04	69%
300	6.70	12.85	65%
360	6.42	12.13	61%
420	6.08	10.92	55%
480	6.11	9.00	45%
Compression			
180	8.22	12.11	23%
240	5.48	12.83	44%
300	4.16	13.02	58%
360	3.20	11.51	68%
420	3.04	10.90	9%
480	3.60	8.98	7%

Table 7 Mechanical behavior of timber scarf joint under various widths

Width (mm)	Displacement (mm)	Initial stiffness (kN/mm)	Degradation
Tension			
120	6.42	12.13	61%
100	7.97	10.09	63%
80	11.52	8.03	68%
Compression			
120	3.20	12.11	23%
100	4.94	10.07	40%
80	8.74	8.02	57%

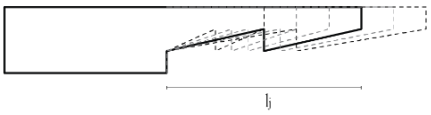

(a) Joint length modification

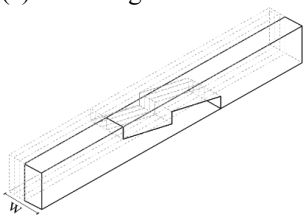

(b) Width modification

Fig. 13 Geometry modification on scarf joint

strengthening elements.

For the geometry modifications, the model was adjusted to explore various sizes of joint length and width (Fig. 13). Traditional guidelines suggest that the joint length should typically be 3 to 4 times the height of the joint. In this parametric analysis, the control length of the joint was set to 360 mm, which corresponds to 3 times the joint width. By modifying the joint length and width while keeping other variables constant, the analysis aims to identify how the geometry of the joint influences its mechanical performance, such as load-bearing capacity, stiffness, and deformation behavior.

Under both tension and compression loads, it was observed that shorter joint lengths led to greater displacement and lower stiffness compared to the control joint length and width (Table 6). This suggests that longer joint areas contribute to improved joint performance, providing enhanced load-bearing capacity and greater stiffness, even though the bearing surfaces between the scarf members remain the same. This aligns with the recommended ratio and dimensions for scarf joints, which suggests a length of 3 to 4 times the joint width.

When considering the width of the timber scarf joint, it was observed that decreasing the width negatively affected joint behavior, resulting in reduced stiffness and higher displacement (Table 7). This reduction in performance can be attributed to the smaller contact area between the connected members. Conversely, increasing the width or height of the joint provides a broader surface area to resist loads, leading to increased strength and stiffness. Both joint length and width are crucial parameters that influence the performance of timber scarf joints. Longer joints offer better structural integrity, while wider joints improve load distribution and enhance overall stiffness and strength.

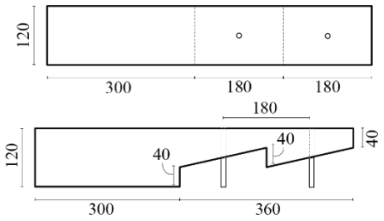

Fig. 14 Model setup for basic scarf joints with dowels

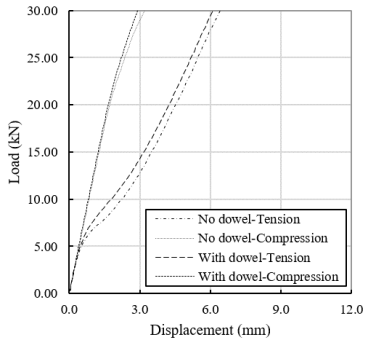

(a) Load-displacement curves of timber scarf joints

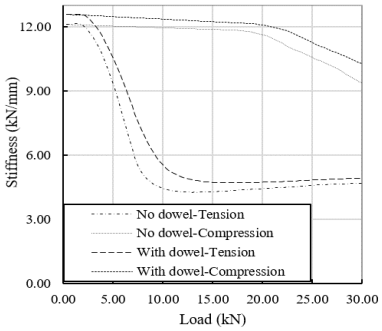

(b) Stiffness degradation curves of timber scarf joints

Fig. 15 (a) Load-displacement curves and (b) stiffness degradation curves for timber scarf joint with and without dowels

4.2 Dowel modifications

4.2.1 Comparison of timber scarf joints with different dimensions

Timber connections are vulnerable to brittle failure, often caused by improper placement of dowel fasteners. Two key factors contributing to this vulnerability are dowel size and spacing, which are interrelated since spacing depends on dowel diameter. In this analysis, the dowel diameter is assumed to be 10 mm (Fig. 14).

The main comparison of dowel modifications is to examine joint performance with and without dowels. This study is similar to the study in validation. The material properties used are C30 softwood for the joint members and D40 hardwood for the dowels, consistent with the analysis of the stop-splayed and tabled scarf joint with key. To enhance comparability, simulation results were compared between the basic scarf joint and Model A (scarf joint with key), and further between Model A and Model B, which includes additional dowels within the joint.

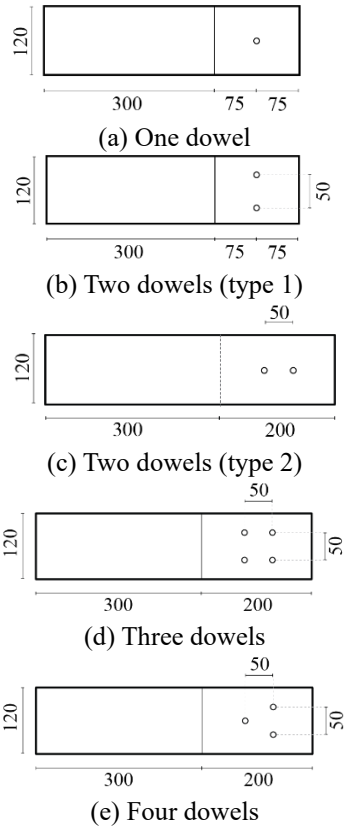

Fig. 16 Joint design with multiple dowels (unit: mm)

The analysis revealed a 5% stiffness difference between basic scarf joints with and without dowels (Fig. 15). This suggests that the scarf joints, which already have bearing surfaces, rely on dowels primarily to prevent the connection from being pulled apart. When comparing Models A and B from the previous section, Model B, which includes dowels, shows a 26% increase in yield load and a 30% increase in stiffness over Model A. This indicates that the joint size significantly affects the necessity of dowels in scarf joints.

In the basic scarf joint, with a 1:1 width-to-height ratio, the bearing contact surfaces play a more critical role in connection strength than the dowels. In contrast, Model A, with a 2:5 width-to-height ratio, benefits more from dowels in terms of mechanical performance. This observation suggests that the ratio of width to height greatly influences the effectiveness of dowels in scarf joints and warrants further analysis for a deeper understanding of the impact on joint performance.

4.2.2 Multiple dowels

It is obvious that the use of dowels more than one in timber connection will increase the strength of the connection. However, in terms of wooden pegs, the influence of the number of dowels might not be fully analyzed in most of previous studies. The impact of multiple dowels is evaluated between the cases of no dowels, one dowel, two dowels, three dowels, and four dowels (Fig. 16).

From the load-displacement curve of this analysis (Figs. 17 and 18), the joint with dowels shows a significant impact

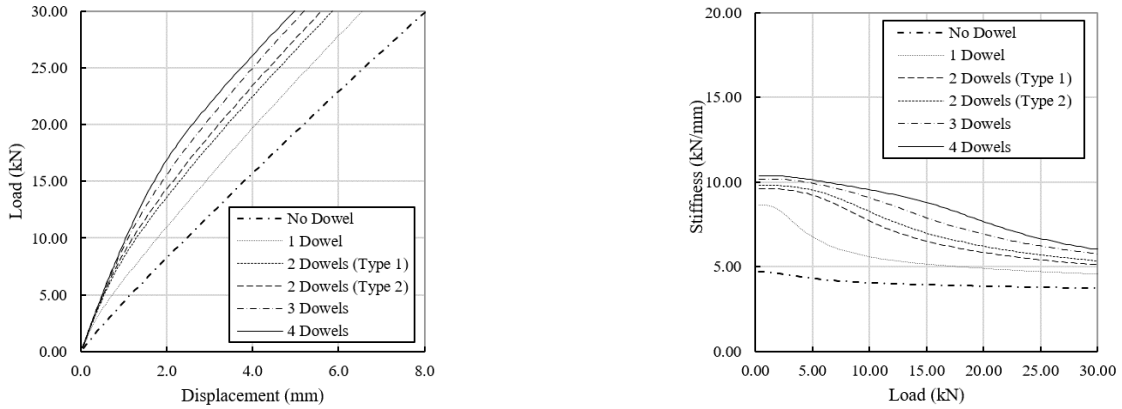

(a) (b)

Fig. 17 (a) Load-displacement curves and (b) stiffness degradation curves for joints with dowels under tension load

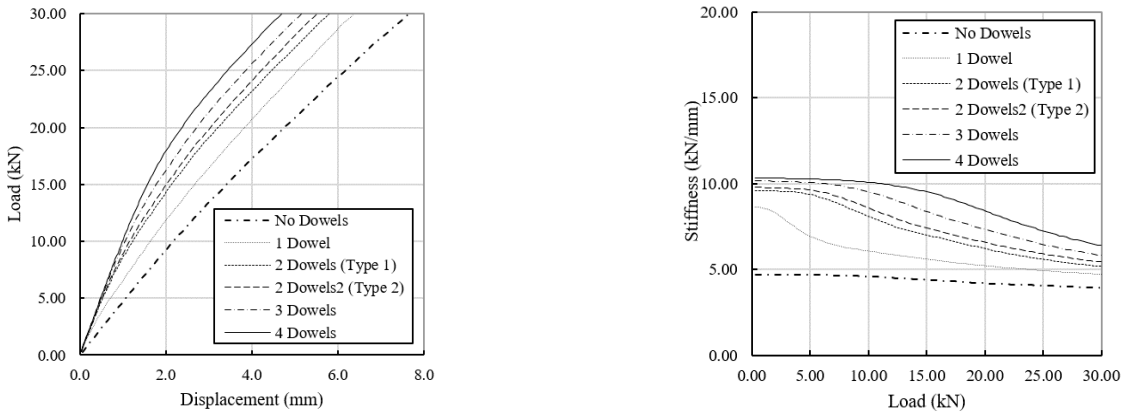

(a) (b)

Fig. 18 (a) Load-displacement curves and (b) stiffness degradation curves for joints with dowels under compression load

on joint strength and stiffness compared to the joint without dowels. The stiffness keeps increasing as the number of dowels increases. When the load is applied to the connections, the decreasing percentage in stiffness is higher for the joint with dowels than without. Under compression and tension loads, joints exhibited greater strength under compression, aligning with the inherent properties of wood as a material.

Another observed behavior is the difference between the two-dowel configurations in Type 1 and Type 2 (refer to Figs. 15(b) and 15(c)). Simulations of the joint under compression and tension reveal that the Type 2 configuration has a higher yield load value than Type 1, as indicated by the stiffness and displacement of the connection. This demonstrates that dowels are more effective when placed parallel to the load direction rather than perpendicular to it. This phenomenon is significant for improving the strength of the connection. Further studies on dowel placement in connections are expected to enhance the performance of timber buildings.

5. Conclusions

The evaluation of stop-splayed and tabled scarf joints with a key, using numerical modeling and validated against experimental results, yielded promising outcomes. The numerical model demonstrated an average accuracy of 69% across three configurations: (1) Model A – basic scarf joint, (2) Model B – scarf joint with wooden pegs, and (3) Model C – scarf joint with steel pins. The yield load from the numerical model was higher than the experimental results, indicating the presence of additional factors influencing the strength of timber scarf joints under tension. Material strength is the primary factor affecting the results, as it does not fully represent the materials used in the experimental tests. Nevertheless, the findings still offer valuable insights into how timber scarf joints can be analyzed through numerical simulations.

In sensitivity analysis, various parameters can be adjusted to evaluate their impact on the simulation results. In terms of connection properties, changes in the material properties of the scarf members had a greater impact on the connection capacity than changes in the key members. Regarding model setup, mesh size had a more significant influence on simulation accuracy than adjustments in load increments and iterations. It is important to note that the most suitable mesh sizes will depend on the size of the numerical model. Further analysis of mesh size and model ratio will be essential to achieve greater accuracy in

numerical modeling using FEA.

The parametric analysis revealed that geometry sizes based on recommended proportions and dimensional limits from the literature yielded the best performance. Longer joint lengths in basic scarf joints resulted in stronger connections. However, narrower joints, in terms of width and height, exhibited weaker connections, likely due to reduced contact areas. Meanwhile, dowels were found to improve the strength of scarf joints, though the effectiveness was more pronounced in scarf joints with a width-to-height ratio of 2:5 compared to those with a 1:1 ratio. Comparing the results between the basic scarf joint and Model A highlights the importance of considering the width and height ratio of the scarf members to determine whether dowels are necessary.

Acknowledgements

This research was supported by National Research Foundation of Korea (No. 2021R1A5A1032433). Also, the work was conducted under the umbrella of the Institute of Information & Communications Technology Planning & Evaluation (IITP) of the Korean government (RS-2021-II211343, MSIT).

References

Ceraldi, C., D'Ambra, C., Lippiello, M., Sandoli, A. and Prota, A. (2021), "Structural behavior of stop-splayed scarf joint reinforced with timber pegs", *Construct. Build. Mater.*, **269**, 121330.

Emile, C., Xiaobin, S., Yajie, W. and Kai, L. (2018), "Lateral performance of mortise-tenon jointed traditional timber frames with wood panel infill", *Eng. Struct.*, **161**, 223-230.

Feio, A.O., Lourenco, P.B. and Machado, J.S. (2014), "Testing and modeling of a traditional timber mortise and tenon joint", *Mater. Struct.*, **47**, 213-225.

Green, D.W., Winandy, J.E. and Kretschmann, D.E. (1999), *Wood handbook: Wood as an Engineering Material*, General Technical Report FPL (GTR-113), USDA Forest Service, Forest Products Laboratory, 4.1-4.45.

Huang, H., Wu, Y., Li, Z., Sun, Z. and Chen, Z. (2018), "Seismic behavior of Chuan-Dou type timber frames", *Eng. Struct.*, **167**, 725-739.

Li, S., Zhou, Z., Luo, H., Milani, G. and Abruzzese, D. (2020), "Behavior of traditional Chinese mortise-tenon joints: Experimental and numerical insight for coupled vertical and reversed cyclic horizontal loads", *J. Build. Eng.*, **30**, 101257.

Li, X., Zhao, J., Ma, G. and Chen, W. (2015), "Experimental study on the seismic performance of a double-span traditional timber frame", *Eng. Struct.*, **98**, 141-150.

National Research Institute of Cultural Heritage in Korea (2014), *Traditional Wooden Building Construction Method*.

Ren, G., Xue, J., Xu, D. and Ma, L. (2021), "Experimental and theoretical analysis on rotation performance of cress-shaped joints with dowel in traditional timber structures", *J. Build. Eng.*, **37**, 102163.

Schmidt, R.J. and Daniels, C.E. (1999), "Design consideration for mortise tenon connections", Department of Civil and Architectural Engineering, University of Wyoming Laramie, Research Report, Hanover, New Hampshire.

Sha, B., Wang, H. and Li, A. (2019), "The influence of the damage of mortise-tenon joint on the cyclic performance of the traditional Chinese timber frame", *Appl. Sci.*, **9**, 3429.

Wu, Y.-J., Wang, L., Lin, H.-S., Zhang, L.-P. and Xie, Q.-F. (2022), "Effect of shear force on the rotational performance of straight mortise-tenon joints", *Structures*, **41**, 501-510.

Xue, J., Song, D., and Wu, C. (2021), "Precise finite element analysis of full-scale straight-tenon joints in ancient timber buildings", *Int. J. Architect. Heritage*, **17**(10), 1-16.

Xue, J., Wu, C., Zhang, X. and Qi, Z. (2020), "Experimental and numerical analysis on seismic performance of straight-tenon joints reinforced with friction damper", *Struct. Control Health Monit.,* **27**, 10

Yang, Q., Yu, Law, P. and Seong, S. (2020), "Load resisting mechanism of the mortise-tenon connection with gaps under in-plane forces and moments", *Eng. Struct.*, **219**, 110755.